Advances in
Bridge Engineering

ORIGINAL INNOVATION

Open Access

Conditional simulation of non-stationary spatially variable ground motions for long-span bridges across non-uniform site conditions

Jubin Lu[1], Liang Hu[2], Zili Xia[3] and Songye Zhu[1*]

*Correspondence:
songye.zhu@polyu.edu.hk

[1] Department of Civil and Environmental Engineering, The Hong Kong Polytechnic University, Kowloon, Hong Kong, China
[2] School of Civil and Hydraulic Engineering, Huazhong University of Science and Technology, Wuhan, Hubei Province, China
[3] Hong Kong-Zhuhai-Macao Bridge Authority, Zhuhai, Guangdong Province, China

Abstract

Non-stationary spatially variable ground motions (SVGMs) are commonly modelled as multivariate oscillatory processes based on evolutionary power spectral density (EPSD) functions. The existing conditional simulation algorithms require the known EPSD functions. The EPSD functions are usually assumed to be identical for all locations, which is unreasonable for long-span bridges because variable soil conditions are practically observed at different bridge piers. This paper proposes a conditional simulation algorithm for non-stationary SVGMs in consideration of non-uniform site conditions. The spatial interpolation tool, termed inverse-distance-weighted (IDW) interpolation, is introduced to estimate the EPSD functions at sites without ground motion measurement. Subsequently, the covariance matrix of the random Fourier coefficients of the multivariate oscillatory processes can be calculated. The Kriging estimation is adopted to obtain the unknown random Fourier coefficients, from which the time histories of the non-stationary SVGMs can be conditionally simulated. The proposed conditional simulation algorithm is first validated through a numerical example, in which the EPSD functions of non-uniform sites are represented by a non-stationary Kanai-Tajimi spectrum with different soil parameters. Then, the algorithm is applied to the Jiuzhou Channel Bridge, a navigation channel bridge of the Hong Kong-Zhuhai-Macau Bridge (HZMB), with complex soil and water conditions. Based on the limited in-situ seismic measurement data, the site characteristics in the bridge area are analysed, and the ground motion time histories at all piers can be generated.

Keywords: Spatially variable ground motions, Non-stationary, Conditional simulation, Non-uniform sites, The Hong Kong-Zhuhai-Macau bridge (HZMB)

1 Introduction

Earthquake ground motions exhibit spatially variable features because of incoherent, wave-passage and site effects (Kiureghian 1996). The spatially variable ground motions (SVGMs) are mainly reflected by the differences in ground motion time histories at various spatial locations. As indicated by previous studies (Zerva and Zervas 2002; Bi et al. 2010, 2011; Li et al. 2018a; Zhong et al. 2018; Kim et al. 2021), SVGMs may have considerable and usually adverse effects on the responses of extended structures, such as long-span bridges. Therefore, various SVGM simulation algorithms have been researched in

the past decades (Hao et al. 1989; Oliveira et al. 1991; Huang and Wang 2015; Wu and Gao 2019; Rodda and Basu 2020; Lu et al. 2021). These algorithms can be divided into two categories, namely, unconditional and conditional simulation algorithms. The former is based on the power spectral density (PSD) function and the spatial coherency model to generate the SVGMs by using the spectral representation method. However, the drawback of the algorithm is that the simulated earthquake time histories are typically inconsistent with the recorded ones at the measured sites.

In contrast, the conditional simulation algorithm can not only simulate the earthquake time histories with spatially variable features but also ensure that the simulated time histories at the measured sites are compatible with the actual earthquake records (Kameda and Morikawa 1992, 1994). Therefore, the conditional simulation can inherit the physical characteristics of the actual earthquakes and thus is more suitable for practical applications (Zerva 2009). The conditional simulation algorithm was first proposed for multivariate stationary processes by Vanmarcke and Fenton (1991). This algorithm uses the Kriging method to estimate the Fourier coefficients of the unmeasured stationary processes based on the covariance matrix of the Fourier coefficients, where the covariance matrix can be derived from the given auto-power spectral density (PSD) functions and a coherency model. However, seismic ground motions often exhibit non-stationary characteristics, which are not reflected in the conditional simulation algorithm proposed by Vanmarcke and Fenton (1991). Vanmarcke, et al. (1993) proposed one solution by dividing ground motion time histories into several time segments and treating each as a stationary process. Another solution is to project the non-stationary processes into the corresponding stationary ones by using the time and frequency modulation functions (Heredia-Zavoni and Santa-Cruz 2000). However, both solutions are based on approximations and assumptions about the non-stationary processes. In view of this, Hu et al. (2012) proposed a new conditional simulation algorithm by modelling non-stationary SVGMs as multivariate oscillatory processes. The proposed algorithm calculates the covariance matrix of the Fourier coefficients by using the evolutionary power spectral density (EPSD) function that preserves the non-stationary characteristic of SVGMs. Afterwards, Cui and Hong (2020) improved the algorithm by solving the ill-condition problem in computing the inversion of the covariance matrix and conducting the bias error analysis of the algorithm.

Regardless of whether the stationary or non-stationary SVGMs are simulated, the above conditional simulation algorithms require the information of the PSD or EPSD functions at all sites and an appropriate coherency model. The latter can adopt the empirical or semi-empirical coherency models (Harichandran and Vanmarcke 1986; Luco and Wong 1986) with the model parameters calibrated with sufficient in-situ earthquake records. The former, commonly assumed identical at all sites, is equal to the PSD or EPSD function computed from the measured record at one specific site. Consequently, the previous studies typically used only a single earthquake record from one site to conduct the conditional simulation. This assumption is reasonable only if all the sites share uniform soil conditions. However, this assumption may cause large errors in the simulated time histories for long-span bridges that usually span multiple sites with different water and soil conditions. In addition, many long-span bridges are equipped with multiple seismographs that measure earthquake records with different PSD or EPSD

functions. As far as we know, how to conduct conditional simulations of SVGMs based on the multiple measured records at non-uniform sites remains an unaddressed question in the literature. Konakli and Der Kiureghian (2012) attempted to estimate the PSD functions at all sites by using the frequency response functions (FRFs) of soil columns with the approximate central frequencies and damping ratios. Bi and Hao (2012) derived the FRF model based on one-dimensional wave propagation theory, which reflects the actual multiple soil columns at sites. Li et al. (2015) simulated the seafloor earthquake ground motions on offshore sites by considering complex soil conditions. Since earthquake ground motions along the piles are very different from those on the ground surface, Li et al. (2018b) further simulated the depth-variable and spatially variable ground motions on heterogeneous onshore and offshore sites. These approaches can reflect the non-uniform site conditions adequately only if the information of the soil profile and the motion characteristic of the bedrock are known. Considering abundant onshore earthquake records are required (Li et al. 2018c), it is usually difficult to obtain all the information accurately in practice.

The spatial interpolation, such as the inverse-distance-weighted (IDW) interpolation, is commonly used to estimate the unmeasured spatial values at the target locations on the basis of the measured spatial values at close locations. It has also been widely used in earthquake engineering to estimate the earthquake-related parameters in the spatial domain. For example, Thráinsson et al. (2000) investigated the performance of the IDW interpolation in estimating the Fourier spectra of the ground motions. The error analysis was comprehensively studied based on the earthquake data from the SMART-1 array. The results showed that the IDW interpolation could achieve satisfactory results in the Fourier spectra at the unmeasured sites if their distances to the measured sites are within 1 km. Suzuki et al. (2017) used the IDW interpolation to estimate the time histories of the M7.3 Kumamoto earthquake at the unmeasured locations. Lu et al. (2021) and Cheng et al. (2021) estimated the response spectra at the target locations by using the IDW interpolation. Then, they generated the corresponding time histories using continuous wavelet transform. The previous studies imply that the PSD or EPSD functions of the unmeasured sites can be estimated using the IDW interpolation.

The major limitations of the above-reviewed literature are summarized as follows: (1) The conditional simulations of SVGMs often assumed that the PSD/EPSD functions at all sites were identical. This assumption was unsuitable for non-uniform site conditions. (2) The simulations usually utilized only one measured record at one specific site and could not consider multiple measurement records at different sites. Consequently, the measured records could not be used adequately in practice. Given these limitations, an improved conditional simulation algorithm for non-stationary SVGMs is proposed in the present study to estimate the EPSD functions at the unmeasured sites by using the IDW interpolation. Compared to the existing conditional simulation algorithms, the proposed algorithm can simulate the SVGMs under non-uniform site conditions and thus is more suitable for long-span bridges that often span various sites with different soil conditions. In addition, the proposed algorithm can simultaneously utilize multiple measurement records at different sites, conforming to the arrangement of multiple seismographs installed in structural health monitoring (SHM) systems for long-span bridges. The proposed algorithm is first validated through a numerical example, in which

the EPSD functions of non-uniform sites are modelled by a non-stationary Kanai-Tajimi spectrum with different soil parameters. The estimated results in the frequency domain, such as the estimated EPSD functions and coherences, are compared with the target ones. The time-domain results are compared with those obtained using the unconditional simulation algorithm (Deodatis 1996), the real EPSD functions of all sites, and the real coherency model. Subsequently, the proposed conditional simulation algorithm is applied to a navigable channel bridge of the Hong Kong-Zhuhai-Macau Bridge (HZMB), namely the Jiuzhou Channel Bridge, situated on sites with complex soil and water conditions. Based on the in-situ measured ground motion records of the M5.2 Yulin earthquake, a complete simulation procedure, including data processing, spectra estimation, coherency model updating, and conditional simulation, is conducted.

The paper is organised as follows: Section 2 introduces the conditional simulation algorithm for non-stationary SVGMs. Section 3 presents the approximation approach of the EPSD functions based on the IDW interpolation. The numerical example and the actual application to the HZMB are conducted in Section 5 to validate the proposed algorithm. Finally, the conclusions are summarised in Section 6.

2 Conditional simulation of the non-stationary SVGMs

2.1 EPSD model

Non-stationary seismic excitations $Y(t)$ can be modelled as a zero-mean Gaussian oscillatory process, which can be expressed as (Priestley 1966, 1967),

$$Y(t) = \int_{-\infty}^{+\infty} A(t,\omega) e^{i\omega t} d\overline{Z}(\omega) \tag{1}$$

where $A(t,\omega)$ is the time and frequency modulation function; $\overline{Z}(\omega)$ is the stationary process with the property of $E\left[d\overline{Z}(\omega)d\overline{Z}(\omega)^*\right] = \overline{S}(\omega)d\omega$, in which $\overline{S}(\omega)$ is the auto-PSD of the stationary processes $\overline{Z}(\omega)$ and "*" stands for a complex conjugate. The corresponding auto-EPSD of the oscillatory process $Y(t)$ can be expressed as,

$$S(\omega,t) = A(t,\omega)\overline{S}(\omega) \tag{2}$$

The cross-EPSD of the two spatially correlated non-stationary processes $Y^j(t)$ and $Y^k(t)$ can be written by introducing a proper coherency model $\gamma^{jk}(\omega)$,

$$S^{jk}(\omega,t) = \sqrt{S^{jj}(\omega,t)S^{kk}(\omega,t)} \cdot \gamma^{jk}(\omega) \tag{3}$$

where j and k are the spatial indicators; $S^{jj}(\omega,t)$ and $S^{kk}(\omega,t)$ are the auto-EPSD of $Y^j(t)$ and $Y^k(t)$, respectively. Then, the time-variant cross-correlation functions $R^{jk}(t_1,t_2)$ of $Y^j(t)$ and $Y^k(t)$ can be derived based on Eq. (3) as,

$$R^{jk}(t_1,t_2) = \int_{-\infty}^{+\infty} S^{jk}(\omega,t) e^{i\omega(t_1-t_2)} d\omega \tag{4}$$

2.2 Conditional simulation based on the kriging algorithm

The non-stationary process $Y(t)$ with a duration T and a sampling rate Δt can be expanded as its Fourier series form,

$$Y(t) = \frac{A_1}{2} + \sum_{n=2}^{N} (A_n \cos \omega_n t + B_n \sin \omega_n t) \tag{5}$$

where N is the order of Fourier series expansion, which should be less than $T/(2\Delta t)$ according to the Nyquist-Shannon sampling theorem. The random Fourier coefficients A_n and B_n can be expressed as,

$$A_n = \frac{2}{T}\int_0^T Y(t) \cos(\omega_n t) dt, \qquad n = 1, 2, \ldots, N \tag{6}$$

$$B_n = \frac{2}{T}\int_0^T Y(t) \sin(\omega_n t) dt, \qquad n = 2, 3, \ldots, N \tag{7}$$

For the multivariate processes, let $\boldsymbol{Y}^O(t) = \left[Y^{O,1}(t)\ Y^{O,2}(t) \cdots Y^{O,m_O}(t)\right]$ and $\boldsymbol{Y}^S(t) = \left[Y^{S,1}(t)\ Y^{S,2}(t) \cdots Y^{S,m_S}(t)\right]$ be the measured processes with the total number m_O and the unmeasured processes with the total number m_S, respectively. Accordingly, their random Fourier coefficients vector can be assembled as $\boldsymbol{F}^O = \left[\left(\boldsymbol{F}^{O,1}\right)^T \left(\boldsymbol{F}^{O,2}\right)^T \cdots \left(\boldsymbol{F}^{O,m_O}\right)^T\right]^T$ and $\boldsymbol{F}^S = \left[\left(\boldsymbol{F}^{S,1}\right)^T \left(\boldsymbol{F}^{S,2}\right)^T \cdots \left(\boldsymbol{F}^{S,m_S}\right)^T\right]^T$, in which $\boldsymbol{F}^{O,j} = \left[A_1^{O,j} A_2^{O,j} \ldots A_N^{O,j} B_1^{O,j} B_2^{O,j} \ldots B_N^{O,j}\right]^T$ (j=1,2, ..., m_O) and $\boldsymbol{F}^{S,k} = \left[A_1^{S,k} A_2^{S,k} \ldots A_N^{S,k} B_1^{S,k} B_2^{S,k} \ldots B_N^{S,k}\right]^T$ (k=1,2,..., m_S), respectively. For example, $A_{20}^{O,5}$ and $B_{20}^{O,5}$ mean the random Fourier coefficients of the 5th measured process expanded at the 20th order, while $A_{25}^{S,10}$ and $B_{25}^{S,10}$ mean the random Fourier coefficients of the 10th unmeasured process expanded at the 25th order.

The measured time histories samples can be denoted as $\boldsymbol{y}^O(t)$ while the unmeasured time history samples can be denoted as $\boldsymbol{y}^S(t)$. The Fourier coefficients vectors of $\boldsymbol{y}^O(t)$ and $\boldsymbol{y}^S(t)$ can be expressed as $\boldsymbol{f}^O$ and $\boldsymbol{f}^S$, respectively. The principle of the Kriging-based conditional simulation is to interpolate $\boldsymbol{f}^S$ based on $\boldsymbol{f}^O$ according to the covariance matrix $\boldsymbol{C}$ between $\boldsymbol{F}^O$ and $\boldsymbol{F}^S$. The covariance matrix $\boldsymbol{C}$ can be expressed as,

$$\boldsymbol{C} = \begin{bmatrix} \boldsymbol{C}_{\boldsymbol{F}^O\boldsymbol{F}^O} & \boldsymbol{C}_{\boldsymbol{F}^O\boldsymbol{F}^S} \\ \boldsymbol{C}_{\boldsymbol{F}^S\boldsymbol{F}^O} & \boldsymbol{C}_{\boldsymbol{F}^S\boldsymbol{F}^S} \end{bmatrix} \tag{8}$$

The covariance matrix $\boldsymbol{C}$ can be calculated based on the time-variant correlation functions expressed as Eq. (4). The expressions of different components in the covariance matrix $\boldsymbol{C}$ are given in the Appendix.

Then, $\boldsymbol{f}^S$ can be estimated unbiasedly based on the Kriging algorithm as,

$$\hat{\boldsymbol{f}}^S = \boldsymbol{C}^T_{\boldsymbol{F}^O\boldsymbol{F}^S} \boldsymbol{C}^{-1}_{\boldsymbol{F}^O\boldsymbol{F}^O} \boldsymbol{f}^O - \boldsymbol{C}^T_{\boldsymbol{F}^O\boldsymbol{F}^S} \boldsymbol{C}^{-1}_{\boldsymbol{F}^O\boldsymbol{F}^O} \tilde{\boldsymbol{f}}^O + \tilde{\boldsymbol{f}}^S \tag{9}$$

where $\hat{\boldsymbol{f}}^S$ is the estimation of $\boldsymbol{f}^S$; $\tilde{\boldsymbol{f}}^O$ and $\tilde{\boldsymbol{f}}^S$ are the unconditionally generated Fourier coefficients vectors, which can be obtained by

$$\begin{Bmatrix} \tilde{\boldsymbol{f}}^O \\ \tilde{\boldsymbol{f}}^S \end{Bmatrix} = \boldsymbol{L} \cdot \boldsymbol{u} \tag{10}$$

where $\boldsymbol{L}\boldsymbol{L}^T = \boldsymbol{C}$, and $\boldsymbol{u}$ is one realization of independent random variables with standard Gaussian distribution. In practice, $\boldsymbol{L}$ can be obtained using the Cholesky decomposition of $\boldsymbol{C}$.

3 Approximation of EPSD based on the IDW interpolation

In the existing conditional simulation algorithm introduced in Section 2, the coherency model $\gamma^{jk}(\omega)$ and the EPSD of all unmeasured processes are assumed to be known. The empirical or semi-empirical coherency models are practically utilized in most situations, provided that the model parameters are calibrated based on in-situ earthquake records (Konakli et al. 2014; Svay et al. 2017; Chen and Hong 2019). However, the EPSD of the unmeasured processes is often difficult to obtain. In most previous studies, the EPSD of the unmeasured processes is assumed to be identical to that of one measured site, i.e., $S^0(\omega,t) = S^{jj}(\omega,t) = S^{kk}(\omega,t)$. Then, Eq. (3) can be simplified as,

$$S^{jk}(\omega,t) = S^0(\omega,t)\cdot\gamma^{jk}(\omega) \tag{11}$$

where $S^0(\omega,t)$ is the EPSD of one measured site, which can be estimated from the in-situ measured records of earthquake time histories.

However, this assumption is no longer applicable if the variable soil conditions are considered. Therefore, the IDW interpolation is used in this study to estimate the EPSD of the unmeasured sites based on those of the measured sites, which can be expressed as,

$$S^{S,k}(\omega,t) = \frac{\sum_{j=1}^{m_O}\frac{1}{d_{jk}^2}S^{O,j}(\omega,t)}{\sum_{j=1}^{m_O}\frac{1}{d_{jk}^2}} \tag{12}$$

where d_{jk} is the distance between the jth measured process $Y^{O,j}(t)$ and the kth unmeasured process $Y^{S,k}(t)$; $S^{O,j}(\omega,t)$ and $S^{S,k}(\omega,t)$ are the EPSD of $Y^{O,j}(t)$ and $Y^{S,k}(t)$ ($j=1,2,\ldots, m_O$; $k=1,2,\ldots, m_S$), respectively.

The EPSD of the unmeasured processes can be estimated based on Eq. (12). Then, the conditional simulation algorithm of non-stationary SVGMs considering non-uniform site conditions can be executed in the following steps:

Step 1: Estimate the EPSD functions $S^{S,k}(\omega,t)$ of the unmeasured processes $Y^{S,k}(t)$ ($k=1,2\ldots, m_S$) by using the IDW interpolation according to Eq. (12);
Step 2: Calculate the cross-EPSD functions $S^{jk}(\omega,t)$ based on Eq. (3);
Step 3: Calculate the cross-correlation functions $R^{jk}(t_1,t_2)$ based on Eq. (4);
Step 4: Compute the covariance of the random Fourier coefficients vectors $\boldsymbol{F}^O$ and $\boldsymbol{F}^S$ based on Eqs. (A.6)-(A.9) and form the covariance matrix $\boldsymbol{C}$ shown as Eq. (8);
Step 5: Generated the Fourier coefficients vector $\tilde{\boldsymbol{f}}^O$ and $\tilde{\boldsymbol{f}}^S$ unconditionally according to Eq. (10);
Step 6: Obtain the conditionally simulated Fourier coefficients vector $\hat{\boldsymbol{f}}^S$ based on the Kriging algorithm according to Eq. (9);
Step 7: Generate the conditionally simulated samples $\boldsymbol{y}^S(t)$ based on Eq. (5).

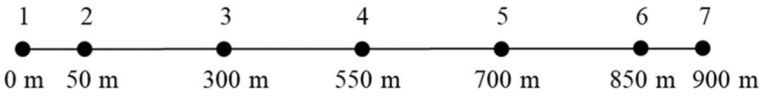

Fig. 1 Site layout

Table 1 Spectrum parameters of all sites

Site No.	Site 1	Site 2	Site 3	Site 4	Site 5	Site 6	Site 7
Distance (m)	0	50	250	450	650	850	900
ω_g (rad/s)	25.13	24.09	19.90	15.71	19.90	24.09	25.13
ξ_g	0.6	0.6	0.6	0.6	0.6	0.6	0.6
$\overline{S}_0$ (cm^2/s^3)	62.30	66.46	83.08	99.70	83.08	66.46	62.30
ω_f (rad/s)	2.51	2.41	1.99	1.57	1.99	2.41	2.51
ξ_g	0.6	0.6	0.6	0.6	0.6	0.6	0.6

4 Numerical validation

4.1 Site layout and soil characteristics

In this section, a numerical example is used to validate the proposed conditional simulation algorithm for non-stationary SVGMs on non-uniform sites. Figure 1 shows the site layout, where the ground motions at sites 1, 4 and 7 are measured while the ground motions at sites 2, 3, 5 and 6 are to be simulated.

The EPSD functions of all sites adopt the non-stationary Kanai-Tajimi spectrum with different parameters, which can be expressed as (Deodatis 1996),

$$S(\omega, t) = |A(t)|^2 \overline{S}(\omega) \tag{13}$$

$$A(t) = a_1 t \exp(-a_2 t) \tag{14}$$

$$\overline{S}(\omega) = \overline{S}_0 \cdot \frac{1 + 4\xi_g^2 \left(\frac{\omega}{\omega_g}\right)^2}{\left[1 - \left(\frac{\omega}{\omega_g}\right)^2\right]^2 + 4\xi_g^2 \left(\frac{\omega}{\omega_g}\right)^2} \cdot \frac{\left(\frac{\omega}{\omega_f}\right)^2}{\left[1 - \left(\frac{\omega}{\omega_f}\right)^2\right]^2 + 4\xi_f^2 \left(\frac{\omega}{\omega_f}\right)^2} \tag{15}$$

where $A(t)$ is the modulation function with parameters $a_1 = 0.906$ and $a_2 = 1/3$; $\overline{S}(\omega)$ is the stationary Kanai-Tajimi spectrum; the spectrum parameters $\overline{S}_0$, ω_g, ξ_g, ω_f, and ξ_f denote the PSD, domain frequency of the foundation soil, damping ratio of the foundation soil, central frequency of the filter, and damping radio of the filter, respectively. These spectrum parameters depend on different soil conditions. In this study, sites 1 and 7 are assumed to be rock or stiff soil whereas site 4 is assumed to be deep cohesionless soil. The spectrum parameters of other sites are assumed to change linearly with the distances from sites 1, 4 and 7. The spectrum parameters of all sites are listed in Table 1.

In addition, the coherencies of the sites are modelled by using the Harichandran-Vanmarcke coherency model (Harichandran and Vanmarcke 1986), which is expressed as,

$$\gamma^{pq}(\omega) = A\exp\left[-\frac{2d_{pq}}{\alpha\theta(\omega)}(1-A+\alpha A)\right] + (1-A)\exp\left[-\frac{2d_{pq}}{\theta(\omega)}(1-A+\alpha A)\right] \tag{16}$$

where $\theta(\omega)=k\{1+[\omega/\omega_0]^b\}^{-1/2}$, $\omega_0=2\pi f_0$, $A=0.736$, $\alpha=0.147$, $k=5210$, $f_0=1.09$, and $b=2.78$; d_{pq} is the distance between any two sites p and q ($p=1,2,\ldots,7$; $q=1,2,\ldots,7$).

4.2 Conditional simulation

Based on the EPSD functions of all sites and the coherency model shown in Eq. (16), the time histories are first simulated using the unconditional simulation algorithm proposed by Deodatis (1996), which are adopted as the measured (reference) time histories for later comparison analysis. The duration T and the time step Δt of the simulated time histories are 10.24 s and 0.01 s, respectively. The unconditionally simulated time histories at sites 1, 4, and 7 are also used as the recorded data in the proposed conditional simulation algorithm. Rather than assuming that all EPSD functions are known and identical, as done in the previous studies, different EPSD functions at sites 1, 4, and 7 are adopted, and the EPSD functions of the other unmeasured sites are estimated based on the IDW interpolation.

Based on the proposed conditional simulation algorithm, the simulated time histories at all sites, which are compatible with the recorded ones at sites 1, 4, and 7, can be obtained. Considering the stochastic characteristic of the simulated samples (Hu et al. 2017), a total of 10,000 samples are generated to obtain a more accurate estimation of EPSD functions and correlation functions. Figure 2 shows only one representative sample. The blue dot lines in the figure denoted as "Simulated" are the conditionally simulated time histories, while the red solid lines denoted as "Target" are the actual time histories obtained from the unconditional simulation algorithm. The simulated time histories are similar to the target ones at sites 2, 3, 5, and 6, indicating that the proposed conditional simulation algorithm can properly generate the time histories of the non-stationary SVGMs.

The correlation functions $R^{pq}(t_1,t_2)$ ($p=1,2,\ldots,7$; $q=1,2,\ldots,7$) of the simulated non-stationary SVGMs can be approximately represented by the ensemble average of the 10,000 sample sets. As shown in Fig. 3, the simulated auto-correlation functions agree well with the target obtained from Eq. (4). It verifies that the proposed conditional simulation algorithm can offer an unbiased estimation of the time-variant auto-correlation functions. Fig. 4 also shows the cross-correlation functions between site 2 and sites 1, 4, and 7 individually. The simulated cross-correlation functions also match the target ones well, indicating that the simulated time history at site 2 is simultaneously compatible with the records at sites 1, 4, and 7. Also, the peak values of the cross-correlation functions reduce with the increasing distance at the same time instant, i.e., $peak(R^{12}) > peak(R^{24}) > peak(R^{27})$ at $t_2=3$ s. The cross-correlation functions between site 3 and sites 1, 4, and 7 show a similar trend. This trend is generally consistent with the expectation.

The EPSD functions at sites 2, 3, 5, and 6 can be estimated based on the simulated time histories by using the Priestley estimation method (Priestley 1965). Figure 5 shows the comparison between the target EPSD functions and the estimated EPSD functions at sites 2 and 3. Here, the estimated EPSD functions are the ensemble average obtained

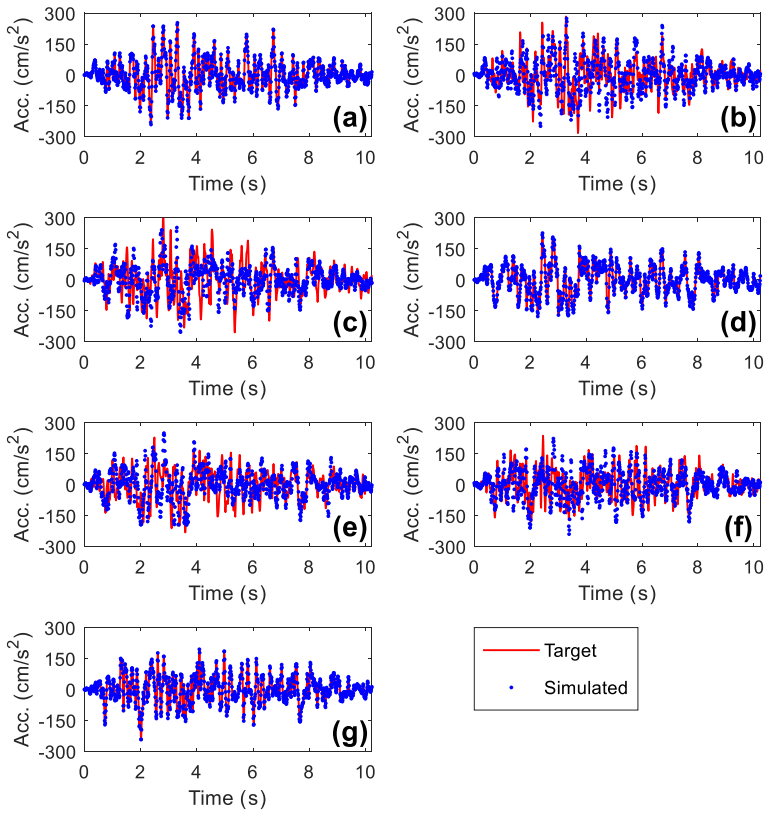

Fig. 2 Comparison between measured/target and simulated time histories at **a** site 1, **b** site 2, **c** site 3, **d** site 4, **e** site 5, **f** site 6, and **g** site 7

from 100 sample sets of the simulated time histories. Figure 6 shows the slices of the EPSD functions at sites 2 and 3, which correspond to $t=3$ s in Fig. 5. In Fig. 6, "One sample" denotes the raw estimation from one representative simulated time histories, "Estimated" denotes the ensemble average from 100 sample sets of the simulated time histories, and "Target" denotes the target one. Figures 5 and 6 show that the simulated time histories at the unmeasured sites are consistent with their target EPSD functions.

Based on the estimated EPSD functions, the estimated coherence $\hat{\gamma}^{pq}(\omega)$ between sites p and q can be calculated as follows,

$$\hat{\gamma}^{pq}(\omega) = \frac{1}{T}\int_0^T \frac{\hat{S}^{pq}(\omega,t)}{\sqrt{\hat{S}^{pp}(\omega,t)\hat{S}^{qq}(\omega,t)}}dt \tag{17}$$

where $\hat{S}^{pq}(\omega,t)$, $\hat{S}^{pp}(\omega,t)$ and $\hat{S}^{qq}(\omega,t)$ denote the estimated cross- and auto-EPSD functions; and T is the time duration.

The unconditional simulation algorithm proposed by Deodatis (1996) exhibited a large error in the imaginary part of the cross-EPSD functions. Thus, only the real part of the cross-EPSD functions is used in Eq. (17). The estimated coherences between site 2 and other sites are shown in Fig. 7. A very good agreement with the target ones can be observed.

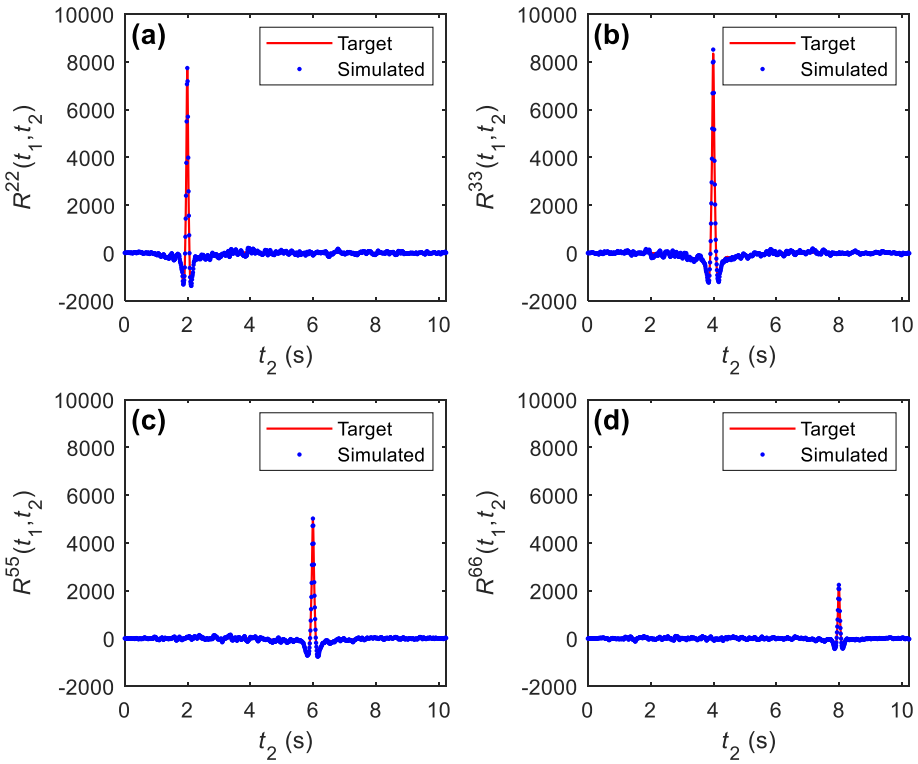

Fig. 3 Comparison of auto-correlation functions in the numerical example: **a** $R^{22}(t_1,t_2)$ at $t_1=2$ s, **b** $R^{33}(t_1,t_2)$ at $t_1=4$ s, **c** $R^{55}(t_1,t_2)$ at $t_1=6$ s, and **d** $R^{66}(t_1,t_2)$ at $t_1=8$ s

Moreover, the acceleration response spectra at unmeasured sites 2, 3, 5, and 6 are estimated based on the average acceleration response spectra obtained from 100 sample sets of the simulated time histories under the damping ratio $\xi=5\%$. The estimated acceleration response spectra are compared with the target ones, which are obtained from the measured time histories generated by the unconditional simulation algorithm. As shown in Fig. 8, the estimated acceleration response spectra are overall closed to those of the target ones, especially when the structural fundamental period T_s is larger than 0.3 s, which corresponds to the period of most long-span bridges. Slight deviations can be observed when the structural fundamental period T_s is around 0.2 s.

5 Application to HZMB

The HZMB is a sea-crossing linking project in south China, connecting Hong Kong Special Administrative Region, Zhuhai City, and Macao Special Administrative Region. The project consists of bridges, artificial islands, and immersed tube tunnels with a total length of 35.6 km. The HZMB crosses sites with different water and soil conditions. The Jiuzhou bridge is one of the navigable channel bridges of the HZMB project. Its elevation view is shown in Fig. 9. To ensure the safety of the bridge, a comprehensive structural health monitoring (SHM) system has been established, including two seismographs installed at the bases of two bridge towers (at sites 3 and 4 in Fig. 9) to record seismic ground excitations acting on the bridge. The proposed conditional simulation algorithm

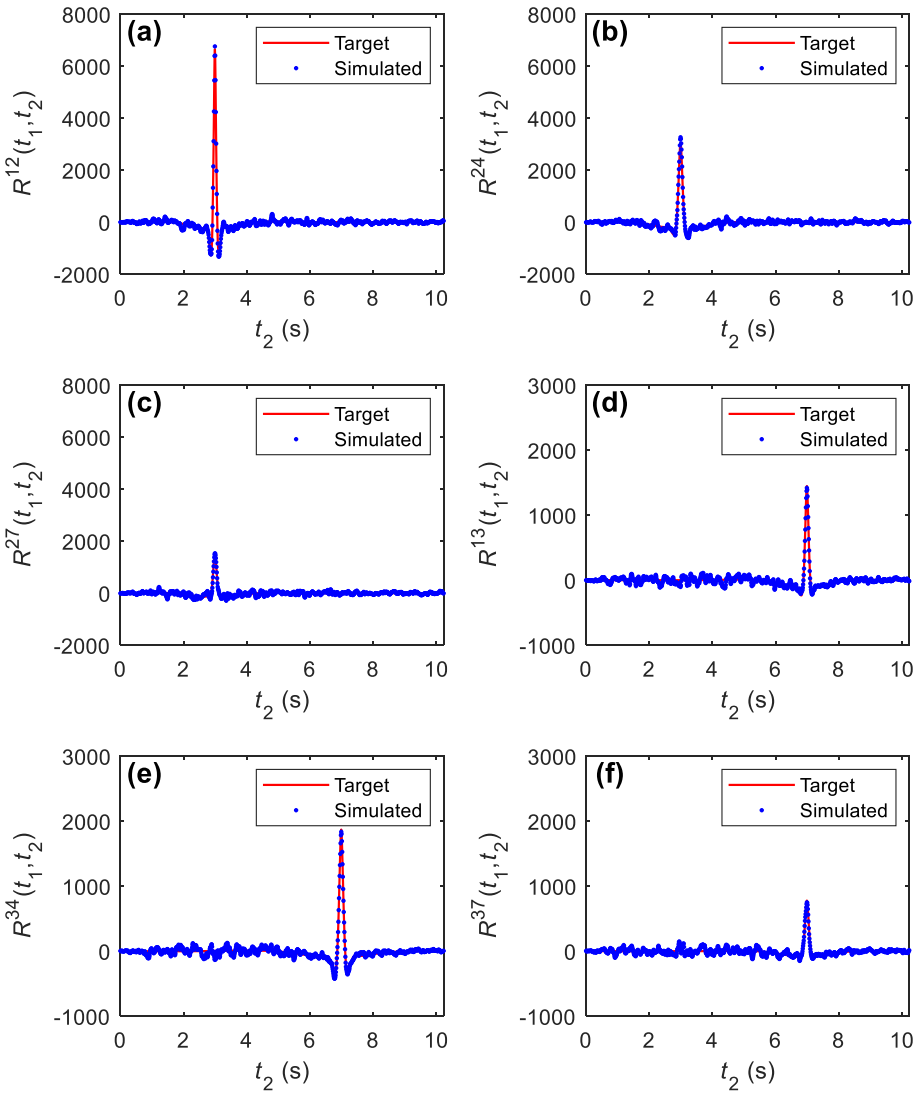

Fig. 4 Comparison of cross-correlation functions in the numerical example: **a** $R^{12}(t_1,t_2)$ at $t_1=3$ s, **b** $R^{24}(t_1,t_2)$ at $t_1=3$ s, **c** $R^{27}(t_1,t_2)$ at $t_1=3$ s, **d** $R^{13}(t_1,t_2)$ at $t_1=7$ s, **e** $R^{34}(t_1,t_2)$ at $t_1=7$ s, and **f** $R^{37}(t_1,t_2)$ at $t_1=7$ s

is adopted to obtain the seismic ground excitations at other unmeasured piers on the basis of the earthquake records measured by the two seismographs, thereby enabling seismic analysis of the Jiuzhou bridge. The non-uniform site conditions in the bridge area are considered in this study.

5.1 Spectra and coherence analysis based on the Yulin earthquake record

The M5.2 Yulin earthquake occurred at 22:55:24 on October 12, 2019. The two seismographs recorded the seismic ground motions at the tower bases during the earthquake. The NS-components of the ground motions are used in this study. The recorded time histories are shown in Fig. 10. The sampling rate is 50 Hz, and the duration of the time histories is around 41 s.

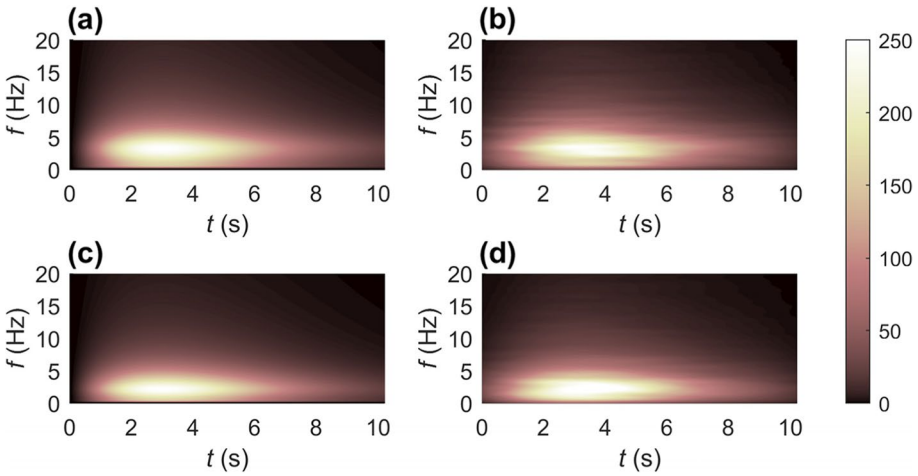

Fig. 5 Comparison of the auto-EPSD functions in the numerical example: **a** the target EPSD at site 2, **b** the estimated EPSD at site 2, **c** the target EPSD at site 3, and **d** the estimated EPSD at site 3

The EPSD functions at sites 3 and 4 can be estimated based on the recorded time histories. The estimated results are shown in Fig. 11 (a)-(b). The EPSD functions at sites 3 and 4 are slightly different, probably because of the non-uniform site conditions. The coherence of the two sites is also analysed. The result shows that the estimated coherence exhibits a large deviation from the Harichandran-Vanmarcke coherency model with its empirical model parameters proposed based on the earthquake records in the SMART-1 array. Therefore, the model parameters of the Harichandran-Vanmarcke coherency model are updated based on the recorded time histories to obtain a suitable in situ coherency model in the Jiuzhou bridge area. The estimated coherence and the updated coherency model are compared in Fig. 11 (c), and the parameters of the calibrated coherency model are listed in Table 2. The coherency model proposed by Harichandran and Vanmarcke (1986) predicts small coherence values at high frequencies and long separation distances. Figure 11 (c) shows that the difference between the estimated coherence and the updated coherency model becomes larger as the frequency increases. The estimated coherence tends to be nearly constant in the high-frequency range. The first reason is that the estimated coherence is biased. The level of bias is related to the duration of the time histories and the bandwidth of the smoothing window used in the spectrum estimation (Zerva 2009). Another possible reason is that the measured earthquake records usually contain high-frequency noise, making it difficult to accurately estimate the coherence in the high-frequency range (Svay et al. 2017).

Based on the estimated EPSD functions at sites 3 and 4 and the updated coherency model, the seismic ground motions on the other unmeasured piers of the Jiuzhou bridge can be obtained according to the proposed conditional simulation algorithm.

5.2 Conditional simulation

Figure 12 shows one sample of the simulated time histories at sites 1, 2, 5, and 6. The simulated time histories at sites 1 and 2 are similar to the measured time history of site

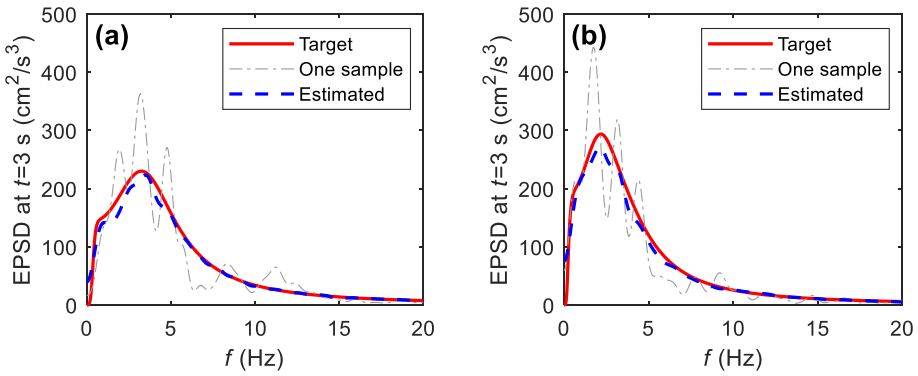

Fig. 6 Comparison of the auto-EPSD function in the numerical example at $t = 3$ s: **a** site 2 and **b** site 3

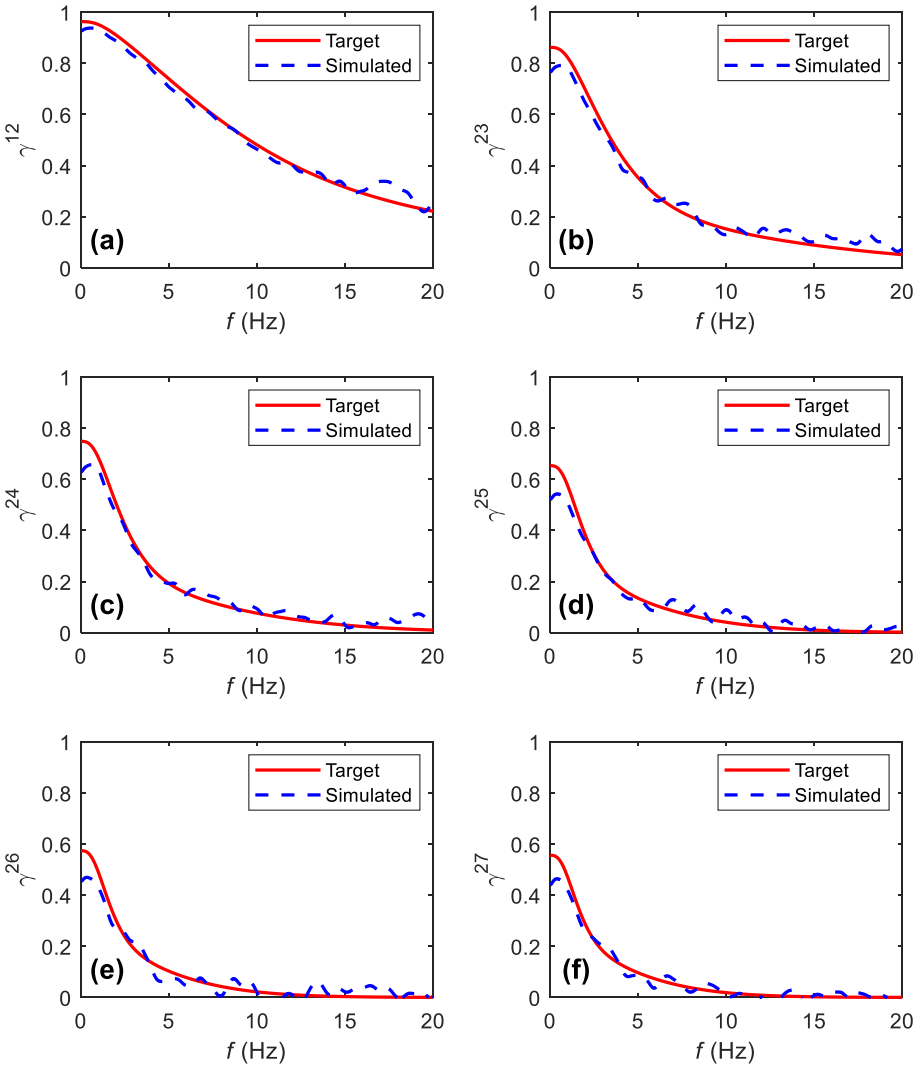

Fig. 7 Comparison between the estimated and target coherences in the numerical example: **a** coherence γ^{12} with $d = 50$ m, **b** coherence γ^{23} with $d = 200$ m, **c** coherence γ^{24} with $d = 400$ m, **d** coherence γ^{25} with $d = 600$ m, **e** coherence γ^{26} with $d = 800$ m, and **f** coherence γ^{27} with $d = 850$ m

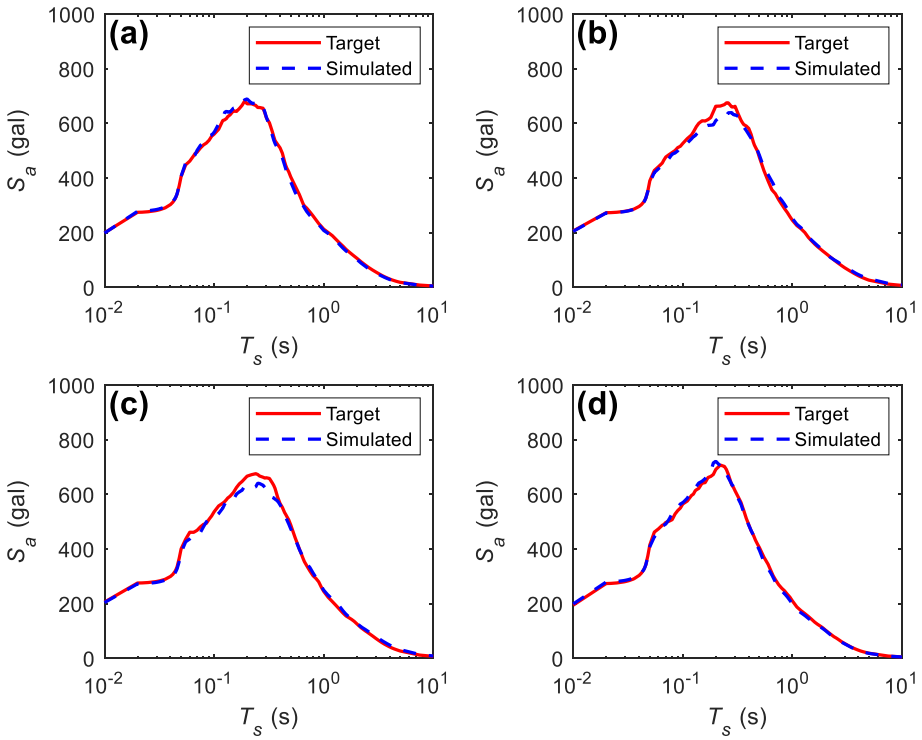

Fig. 8 Comparison of the acceleration response spectra in the numerical example: **a** site 2, **b** site 3, **c** site 5, and **d** site 6

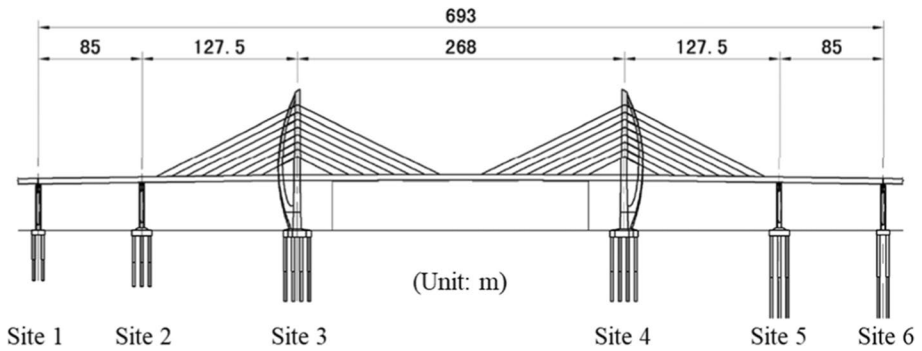

Fig. 9 Elevation view of the Jiuzhou bridge

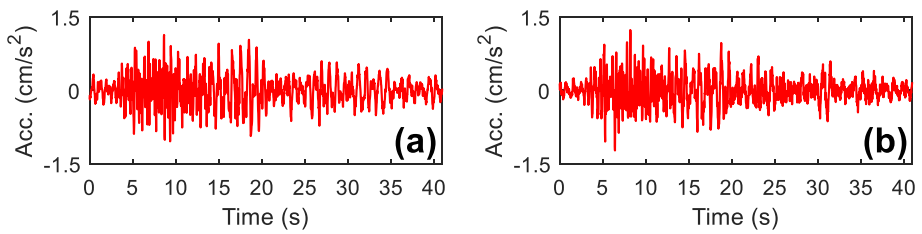

Fig. 10 Measured earthquake time histories at the tower bases of the Jiuzhou bridge: **a** site 3 and **b** site 4

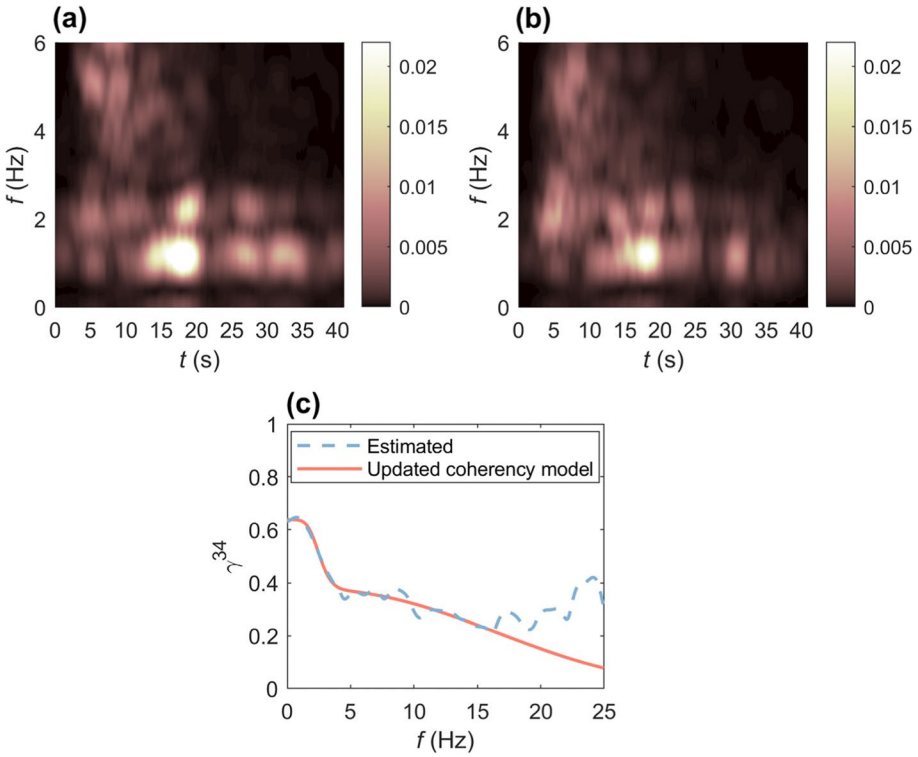

Fig. 11 Spectra and coherence analysis based on the measured earthquake data in the Jiuzhou bridge case: **a** the estimated EPSD at site 3, **b** the estimated EPSD at site 4, and **c** the estimated coherence between sites 3-4 and the updated coherency model

Table 2 Parameters of the updated coherency model

A	a	k	f_0	b
0.586	0.003	131,750	1.489	4.681

3, whereas the simulated time histories at sites 5 and 6 are more similar to the measured time history of site 4. The reason is that the coherence of the two ground motions reduces with the increase in their spatial distance.

The EPSD functions of sites 1, 2, 5, and 6 can also be estimated based on the 100 sample sets of the simulated time histories. Their ensemble averages are shown in Fig. 13. The estimated EPSD functions vary from site 1 to site 6, indicating that the proposed conditional simulation algorithm considers the non-uniform site condition. Afterwards, the coherences can be estimated based on Eq. (17). Figure 14 shows the coherences between site 1 and the other sites. As shown in Fig. 14, the estimated coherences are overall close to the target ones, especially within the frequency range from 0.5 to 5 Hz, where the main excitation energy is concentrated.

The earthquake time histories at the other piers of the HZMB can also be simulated by using the proposed conditional simulation algorithm. However, it should

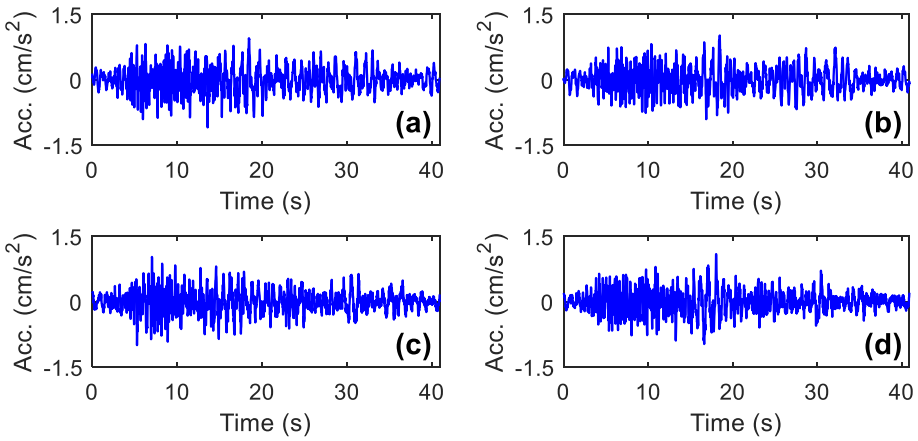

Fig. 12 Simulated earthquake time histories at **a** site 1, **b** site 2, **c** site 5, and **d** site 6 of the Jiuzhou bridge

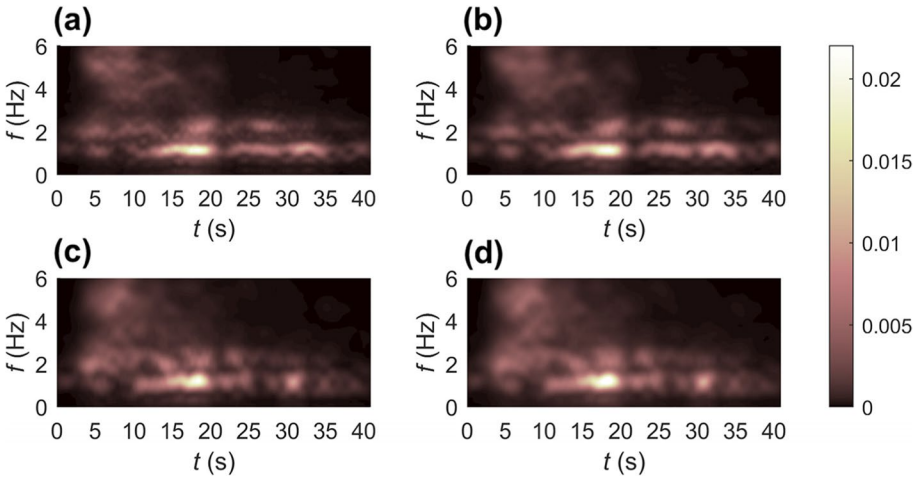

Fig. 13 EPSD of the simulated earthquake time histories at **a** site 1, **b** site 2, **c** site 5, and **d** site 6 of the Jiuzhou bridge

be pointed out that the covariances of the random Fourier coefficients are relatively small when the separation distances between the measured and unmeasured sites are large. As a result, the first two terms on the right side of Eq. (9) become relatively small compared to the third term, and thus the conditional simulation reduces to the unconditional simulation at a large separation distance. Therefore, this study only generates the earthquake time histories at the six piers in the Jiuzhou bridge.

According to the previous studies on the spatial coherency of the SVGMs and the estimated coherences based on the Yulin earthquake records in this study, the spatial coherency becomes very weak and ignorable, if the separation distance is large than 2.5 km. Therefore, it is unnecessary to consider the spatial coherency in the whole area of the super-long bridge. Considering that there are only limited seismographs installed on the HZMB and the HZMB can be divided into multiple segments by expansion joints, it is recommended to conduct the conditional simulation for different segments individually according to the actual situations so that the seismic

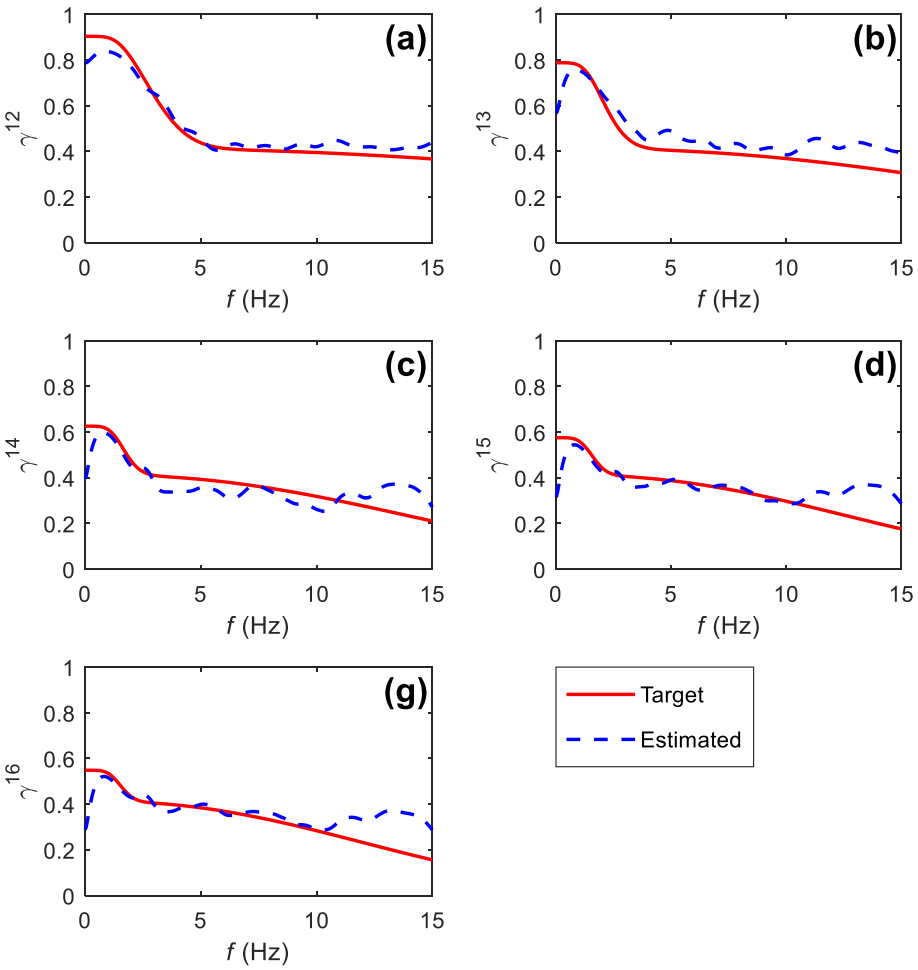

Fig. 14 Comparison between the estimated and target coherences in the Jiuzhou bridge case: **a** Coherence γ^{12} with d = 85 m, **b** Coherence γ^{13} with d = 212.5 m, **c** Coherence γ^{14} with d = 480.5 m, **d** Coherence γ^{15} with d = 608 m, and **e** Coherence γ^{16} with d = 693 m

responses analysis of a super-long bridge can be performed individually for each segment.

6 Conclusions

This paper proposed a conditional simulation algorithm for non-stationary SVGMs with consideration of non-uniform site conditions practically observed for long-span bridges. By modelling non-stationary SVGMs as the multivariate oscillatory processes represented by the EPSD functions, the non-stationary characteristic can be preserved without any assumption on modulation functions. The EPSD functions of the unmeasured sites are estimated using the IDW interpolation based on those of the near sites; consequently, the non-uniform site conditions are taken into account in the conditional simulation algorithm. The numerical example is used to verify the algorithm, wherein the EPSD functions of the non-uniform sites are modelled by a non-stationary Kanai-Tajimi spectrum with different soil parameters. The observations obtained from the numerical example are summarised as follows:

1. The comparison analysis of the time histories and correlation functions implies that the proposed conditional simulation algorithm can generate the time histories of the SVGMs compatible with the measured ones and the non-stationary characteristic can be well reflected.
2. The estimated EPSD functions of the unmeasured sites obtained from the ensemble averages are consistent with the target ones, although the raw estimations obtained from one sample show fluctuation around the target ones. It indicates that the conditional simulation algorithm produces the unbiased estimated EPSD and the performance of the IDW is satisfactory.
3. The ground motion-related parameters like coherence and response spectra calculated from the simulated time histories agree well with the target ones.

The conditional simulation algorithm is further applied to the Jiuzhou bridge situated on sites with complex soil and water conditions. The NS-components of the M5.2 Yulin earthquake measured by the two seismographs at the tower bases are used as the measured data in the conditional simulation. The complete simulation procedure, including data processing, spectra estimation, coherency model updating, and conditional simulation, is executed. The simulated ground motions at the bridge piers will provide guidance for the reconstruction of the ground motion time histories for the entire sea-crossing HZMB in the future.

Appendix

The expression of the covariance matrix $\boldsymbol{C}$ shown in Eq. (8) is recalled,

$$\boldsymbol{C} = \begin{bmatrix} \boldsymbol{C}_{\boldsymbol{F}^O\boldsymbol{F}^O} & \boldsymbol{C}_{\boldsymbol{F}^O\boldsymbol{F}^S} \\ \boldsymbol{C}_{\boldsymbol{F}^S\boldsymbol{F}^O} & \boldsymbol{C}_{\boldsymbol{F}^S\boldsymbol{F}^S} \end{bmatrix} \tag{A.1}$$

where $\boldsymbol{C}_{\boldsymbol{F}^O\boldsymbol{F}^O}$, $\boldsymbol{C}_{\boldsymbol{F}^S\boldsymbol{F}^S}$, $\boldsymbol{C}_{\boldsymbol{F}^O\boldsymbol{F}^S} = \boldsymbol{C}^T_{\boldsymbol{F}^S\boldsymbol{F}^O}$ stand for the covariance matrices of between the random Fourier coefficients vectors $\boldsymbol{F}^O$ and $\boldsymbol{F}^O$, $\boldsymbol{F}^S$ and $\boldsymbol{F}^S$, $\boldsymbol{F}^O$ and $\boldsymbol{F}^S$, respectively. The random Fourier coefficients vectors $\boldsymbol{F}^O$ and $\boldsymbol{F}^S$ can be expressed as,

$$\boldsymbol{F}^O = \left[\left(\boldsymbol{F}^{O,1}\right)^T \left(\boldsymbol{F}^{O,2}\right)^T \cdots \left(\boldsymbol{F}^{O,m_O}\right)^T \right]^T \tag{A.2}$$

$$\boldsymbol{F}^S = \left[\left(\boldsymbol{F}^{S,1}\right)^T \left(\boldsymbol{F}^{S,2}\right)^T \cdots \left(\boldsymbol{F}^{S,m_S}\right)^T \right]^T \tag{A.3}$$

$$\boldsymbol{F}^{O,j} = \left[A_1^{O,j} A_2^{O,j} \ldots A_N^{O,j} B_1^{O,j} B_2^{O,j} \ldots B_N^{O,j} \right]^T \ (j = 1, 2 \ldots, m_O) \tag{A.4}$$

$$\boldsymbol{F}^{S,k} = \left[A_1^{S,k} A_2^{S,k} \ldots A_N^{S,k} B_1^{S,k} B_2^{S,k} \ldots B_N^{S,k} \right]^T \ (k = 1, 2 \ldots, m_S) \tag{A.5}$$

where the superscript denotes the spatial indicator, while the subscript denotes the frequency indicator. Without loss of generality, let A_p^j, A_q^k, B_p^j and B_q^k be the random

Fourier coefficients at different spatial locations and frequency orders. Their covariance can be derived as,

$$E\left(A_p^j A_q^k\right) = \frac{4}{T^2}\int_0^T\int_0^T R^{jk}(t_1,t_2)\cos\omega_p t_1 \cos\omega_q t_2 dt_1 dt_2 \tag{A.6}$$

$$E\left(A_p^j B_q^k\right) = \frac{4}{T^2}\int_0^T\int_0^T R^{jk}(t_1,t_2)\cos\omega_p t_1 \sin\omega_q t_2 dt_1 dt_2 \tag{A.7}$$

$$E\left(B_p^j A_q^k\right) = \frac{4}{T^2}\int_0^T\int_0^T R^{jk}(t_1,t_2)\sin\omega_p t_1 \cos\omega_q t_2 dt_1 dt_2 \tag{A.8}$$

$$E\left(B_p^j B_q^k\right) = \frac{4}{T^2}\int_0^T\int_0^T R^{jk}(t_1,t_2)\sin\omega_p t_1 \sin\omega_q t_2 dt_1 dt_2 \tag{A.9}$$

where $R^{jk}(t_1,t_2)$ is the time-variant cross-correlation functions, which can be calculated based on Eq. (4).

Then, the covariance of the random Fourier coefficients vectors $\boldsymbol{F}^O$ and $\boldsymbol{F}^S$ can be obtained using Eqs. (A.6)-(A.9).

Authors' contributions

All authors have read and approved the manuscript. J. Lu: Methodology, Validation, Formal analysis, Data Curation, Writing - Original Draft, Visualization; L. Hu: Conceptualization, Methodology, Software; Z. Xia: Resources, Project Administration; S. Zhu: Conceptualazation, Investigtion, Writing – Review & Editing, Supervision, Project administration, Funding acquisition.

Funding

The authors are grateful for the financial support from the National Key Research and Development Program of China (Grant No. 2019YFB1600700), the National Observation and Research Station of Material Corrosion and Structural Safety of Hong Kong-Zhuhai-Macao Bridge in Guangdong, the Research Grants Council of Hong Kong through the GRF Project (Grant No. PolyU 152246/18E) and the CRF project (Grant No. C7038-20G), and the Hong Kong Polytechnic University (Grant Nos. ZE2L, ZVX6). The findings and opinions expressed in this paper are solely those of the authors and do not represent the view of the sponsors.

Availability of data and materials

All data generated or analysed during this study are included in this published article.

Declarations

Competing interests

The authors declare that they have no known competing financial interests or personal relationships that could have appeared to influence the work reported in this paper.

Received: 27 May 2022 Accepted: 24 July 2022
Published online: 19 August 2022

References

Bi K, Hao H, Ren W (2010) Response of a frame structure on a canyon site to spatially varying ground motions. Struct Eng Mech 36:111–127

Bi K, Hao H, Chouw N (2011) Influence of ground motion spatial variation, site condition and SSI on the required separation distances of bridge structures to avoid seismic pounding. Earthquake Eng Struct Dynamics 40:1027–1043

Bi K, Hao H (2012) Modelling and simulation of spatially varying earthquake ground motions at sites with varying conditions. Probabilistic Eng Mech 29:92–104

Chen Q, Hong N (2019) Depth coherency analysis for strong seismic motions from KiK-net. J Earthq Eng 25:1762–1787

Cheng Q, Tian Y, Lu X, Huang Y, Ye L (2021) Near-real-time prompt assessment for regional earthquake-induced landslides using recorded ground motions. Comput Geosci 149:1–11

Cui XZ, Hong HP (2020) Conditional simulation of spatially varying multicomponent nonstationary ground motions: Bias and ill condition. J Eng Mech 146:1–13
Deodatis G (1996) Non-stationary stochastic vector processes: seismic ground motion applications. Probabilistic Eng Mech 11:149–167
Hao H, Oliveira CS, Penzien J (1989) Multiple-station ground motion processing and simulation based on smart-1 array data. Nucl Eng Des 111:293–310
Harichandran RS, Vanmarcke EH (1986) Stochastic variation of earthquake ground motion in space and time. J Eng Mech 112:154–174
Heredia-Zavoni E, Santa-Cruz S (2000) Conditional simulation of a class of nonstationary space-time random fields. J Eng Mech 126:398–404
Hu L, Xu YL, Zheng Y (2012) Conditional simulation of spatially variable seismic ground motions based on evolutionary spectra. Earthq Eng Struct Dyn 41:2125–2139
Hu L, Xu Z, Xu YL, Li L, Kareem A (2017) Error analysis of spatially varying seismic ground motion simulation by spectral representation method. J Eng Mech 143:1–13
Huang D, Wang G (2015) Stochastic simulation of regionalized ground motions using wavelet packets and cokriging analysis. Earthq Eng Struct Dyn 44:775–794
Kameda H, Morikawa H (1992) An interpolating stochastic process for simulation of conditional random fields. Probabilistic Eng Mech 7:243–254
Kameda H, Morikawa H (1994) Conditioned stochastic processes for conditional random fields. J Eng Mech 120:855–875
Kim T, Kwon O-S, Song J (2021) Seismic performance of a long-span cable-stayed bridge under spatially varying bidirectional Spectrum-compatible ground motions. J Struct Eng 147:1–19
Kiureghian AD (1996) A coherency model for spatially varying ground motions. Earthq Eng Struct Dyn 25:99–111
Konakli K, Der Kiureghian A (2012) Simulation of spatially varying ground motions including incoherence, wave-passage and differential site-response effects. Earthq Eng Struct Dyn 41:495–513
Konakli K, Der Kiureghian A, Dreger D (2014) Coherency analysis of accelerograms recorded by the UPSAR array during the 2004 Parkfield earthquake. Earthq Eng Struc Dyn 43:641–659
Li C, Hao H, Li H, Bi K (2015) Theoretical modeling and numerical simulation of seismic motions at seafloor. Soil Dyn Earthq Eng 77:220–225
Li C, Li H, Hao H, Bi K, Chen B (2018a) Seismic fragility analyses of sea-crossing cable-stayed bridges subjected to multi-support ground motions on offshore sites. Eng Struct 165:441–456
Li C, Li H, Hao H, Bi K, Tian L (2018b) Simulation of multi-support depth-varying earthquake ground motions within heterogeneous onshore and offshore sites. Earthq Eng Eng Vib 17:475–490
Li C, Li H, Hao H, Bi K (2018c) Simulation of spatially varying seafloor motions using onshore earthquake recordings. J Eng Mech 144:1–14
Lu X, Cheng Q, Tian Y, Huang Y (2021) Regional ground-motion simulation using recorded ground motions. Bull Seismol Soc Am 111:825–838
Luco JE, Wong HL (1986) Response of a rigid foundation to a spatially random ground motion. Earthq Eng Struct Dyn 14:891–908
Oliveira CS, Hao H, Penzien J (1991) Ground motion modeling for multiple-input structural analysis. Struct Saf 10:79–93
Priestley MB (1965) Evolutionary spectra and non-stationary processes. J R Stat Soc Ser B Methodol 27:204–229
Priestley MB (1966) Design relations for non-stationary processes. J R Stat Soc Ser B Methodol 28:228–240
Priestley MB (1967) Power spectral analysis of non-stationary random processes. J Sound Vib 6:86–97
Rodda GK, Basu D (2020) Spatially correlated vertical ground motion for seismic design. Eng Struct 206:1–22
Suzuki W, Aoi S, Kunugi T, Kubo H, Morikawa N, Nakamura H, Kimura T, Fujiwara H (2017) Strong motions observed by K-NET and KiK-net during the 2016 Kumamoto earthquake sequence. Earth Planets Space 69:1–12
Svay A, Perron V, Imtiaz A, Zentner I, Cottereau R, Clouteau D, Bard PY, Hollender F, Lopez-Caballero F (2017) Spatial coherency analysis of seismic ground motions from a rock site dense array implemented during the Kefalonia 2014 aftershock sequence. Earthq Eng Struct Dyn 46:1895–1917
Thráinsson H, Kiremidjian AS, Winterstein SR (2000) Modeling of earthquake ground motion in the frequency domain. John A. Blume Earthquake Engineering Center Rep No 134, Dept of Civil and Environmental Engineering, Stanford Univ, Stanford
Vanmarcke EH, Fenton GA (1991) Conditioned simulation of local fields of earthquake ground motion. Struct Saf 10:247–264
Vanmarcke EH, Heredia-Zavoni E, Fenton GA (1993) Conditional Simulation of Spatially Correlated Earthquake Ground Motion. J Eng Mech 119:2333–2352
Wu Y, Gao Y (2019) A modified spectral representation method to simulate non-Gaussian random vector process considering wave-passage effect. Eng Struct 201:1–15
Zerva A (2009) Spatial variation of seismic ground motions: molldeing and engineering application. CRC Press, Boca Raton
Zerva A, Zervas V (2002) Spatial variation of seismic ground motions: an overview. Appl Mech Rev 55:271–297
Zhong J, Jeon J-S, Ren W-X (2018) Risk assessment for a long-span cable-stayed bridge subjected to multiple support excitations. Eng Struct 176:220–230

Publisher's Note